Optical response of Luttinger semimetals in the normal and superconducting states

Igor Boettcher*
Joint Quantum Institute, University of Maryland, College Park, Maryland 20742, USA

(Received 28 December 2018; published 25 March 2019)

We investigate the optical response properties of three-dimensional Luttinger semimetals with the Fermi energy close to a quadratic band touching point. In particular, in order to address recent experiments on the spectroscopy of pyrochlore iridates and half-Heusler superconductors, we derive expressions for the optical conductivity in both the normal and general superconducting states in the linear response regime within the random phase approximation. The response functions can be decomposed into contributions from intraband and interband transitions, the latter comprising a genuine signature of the quadratic band touching point. We demonstrate the importance of interband transitions in the optical response in the normal state both in the homogeneous and quasistatic limit. Our analysis reveals a factorization property of the homogeneous conductivity in the spatially anisotropic case and the divergence of the conductivity for strong spatial anisotropy. In the quasistatic limit, the response is dominated by interband transitions and significantly different from systems with a single parabolic band. As an applications of the formalism in the superconducting state we compute the optical conductivity and superfluid density for the *s*-wave singlet superconducting case for both finite and vanishing chemical potential.

DOI: 10.1103/PhysRevB.99.125146

I. INTRODUCTION

Ignited by recent advances in growth and characterization of novel classes of spin-orbit coupled materials, the study of many-body physics in three-dimensional Luttinger semimetals with the Fermi energy close to an inverted quadratic band touching (QBT) point is part of the forefront of both theoretical and experimental research on quantum materials. Already in the noninteracting case these systems are highly compelling, as applying strain or quantum confinement can induce a topological insulator state, which furthermore is robust against weak perturbations [1]. An even richer manifold of possible macroscopic phases emerges when considering the effects of long-range or sufficiently strong short-range interactions. Some of the currently most actively investigated platforms for exploring interactions in QBT systems are pyrochlore iridates [2] and half-Heusler superconductors [3,4]. In particular, two recent measurements of their intriguing conductance properties constitute the motivation for the present work [5,6].

What makes the study of many-body physics and interactions in Luttinger semimetals so fascinating can be attributed to two main features. First, as realized by Abrikosov, the long-range Coulomb repulsion between electrons at the QBT point induces a non-Fermi liquid (NFL) phase of the system [7–9]. Although the ultimate stability of this phase is currently still debated, as emergent strong short-range interactions may eventually drive the system into a topological Mott insulator state [10–13], it is fairly certain that correlation functions will show anomalous scaling over some extended range of experimental parameters such as temperature, momentum, and frequency. Second, since the electrons occupying the QBT point carry an effective spin of 3/2, many novel and often tensorial order parameters can be constructed close to the touching point [14–35]. Fortunately both magnetic and superconducting orders of this type are, respectively, covered by the pyrochlore iridates and half-Heusler compounds in experiment.

Pyrochlore iridates, having structural formula $R_2Ir_2O_7$ (denoted *R*-227 for short) with *R* a rare-earth element, have been shown to host a QBT point at the Fermi energy both via theoretical calculations [2] and experimental ARPES studies [36,37]. Most members of the material class show a transition to an insulating phase with octupolar magnetic order at temperatures around 100 K [38]. However, the critical temperature is reduced for Nd-227, and no finite-temperature transition has been observed in Pr-227. Furthermore, Pr-227 may be close to a quantum critical point as a function of ionic radius of *R*, implying that its high temperature phase lies in the corresponding critical fan and thus shows nontrivial scaling of observables as a function of temperature.

A recent THz spectroscopy study [5] by the Armitage group on the optical response of Pr-227 in the normal phase revealed a large additive anomalous contribution to the dielectric function compared to the Drude formula, which can be traced theoretically to originate from interband transitions between the upper and lower bands of the QBT point by Broerman's formula [39]. The determination of the scattering rate shows a $\tau^{-1} \propto T^2$ temperature dependence, however, with an unusually large prefactor indicating that the system may be strongly coupled in the normal phase. The presence of a finite Fermi energy $E_F > 0$ (measured from the QBT point) in the experiment sets a limit on the intermediate frequency and temperature ranges where nontrivial scaling such as Abrikosov's NFL behavior could be observed. Measuring

*iboettch@umd.edu

at larger frequencies or higher temperatures (both compared to E_F), or minimizing E_F directly, will allow us to experimentally test whether the NFL phase is achieved in the normal phase of Pr-227, and thus shed light onto other QBT systems where long-range interactions are important. This clearly calls for a fresh and extended view on the frequency and temperature dependence of the optical conductivity in Luttinger semimetals. Note that the existence of plasmon excitations in the normal state has recently been addressed in Ref. [40].

In half-Heusler superconductors the presence of a QBT point close to the Fermi energy is supported by extensive density functional calculations of the band structure [4]. (A small linear admixture to the QBT is generally expected due to the noncentrosymmetric crystal structure [20], but its effect on the low-energy physics can be estimated to be subleading for realistic E_F [27].) Importantly, several compounds have an inverted band structure and become superconducting at temperatures around 1 K [3,41–43]. Given the low density in these materials, reflected by a small value of E_F, such critical temperatures need to be considered high and seem to require a more complex mechanisms than phonon mediated attraction [19].

The case for unconventional superconductivity in the half-Heuslers was strengthened enormously by a recent measurement of the London penetration depth in YPtBi [6] by the Paglione group, which shows an almost linear temperature dependence of the observable at low temperatures $T/T_c \sim 0.1$, and thereby indicates the presence of line nodes in the gap. Whereas this eliminates the possibility for a pure s-wave gap, the spin-3/2 nature of the fermions at the QBT point allows us to construct many other pairing channels (with or without even-odd-parity mixing) that feature line nodes. Since the associated orders are typically tensorial in nature, an angular resolved measurement of the optical properties appears to be a first step towards eliminating certain candidate orders. More generally, a solid understanding of how distinct superconducting orders contribute to the frequency and directional dependence of the optical conductivity in Luttinger semimetals could be central to discerning which pattern is realized in a given material in future experiments.

The scope of this work is therefore to set up a framework for studying the optical response of Luttinger semimetals in the normal and superconducting phase that allows us to address the challenges described above and support future experimental explorations of QBT systems. We use a purely field theoretic approach starting from the path integral to arrive at the optical conductivity in the linear response regime within the random phase approximation (RPA). In particular, we formulate the theory such as to allow for the complex and unconventional superconducting orders that are possible in the system. We recover the expressions for the longitudinal response in the normal state of Ref. [39] and extend these works by addressing anisotropic corrections, gauge invariance, transverse response, and momentum dependence of response functions. We derive general formulas for the response functions in superconductors with a QBT point and apply them to the s-wave singlet superconductor as a proof of principle. Since the experiments for superconducting YPtBi are in the clean limit [41], we do not consider the effects of disorder in the present work.

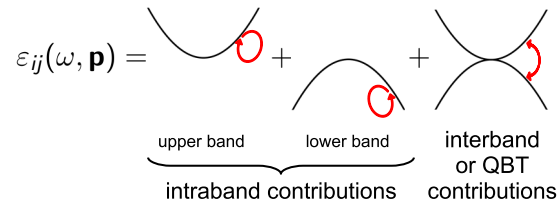

FIG. 1. The contributions to the dielectric tensor $\varepsilon_{ij}(\omega, \mathbf{p})$ can be split into three parts. The first two arise from intraband transitions within, respectively, the upper or lower band, and as such can be computed without knowledge of the other bands. In contrast, interband transitions or genuine QBT contributions are not captured by a single-band model. They encode, however, many important physical features of Luttinger semimetals. For instance, in the normal state they lead to a divergent contribution at low frequency as $E_F \to 0$, or they contain the response from Bogoliubov Fermi surfaces in certain time-reversal symmetry breaking superconducting states—a feature entirely absent in single band systems.

The picture that appears on the RPA level, and which underlies the interpretation of the experiments in Ref. [5], is illustrated in Fig. 1. The optical response functions, given by the dielectric tensor $\varepsilon_{ij}(\omega, \mathbf{p})$ or conductivity tensor $\sigma_{ij}(\omega, \mathbf{p})$, decompose into a sum of intraband and interband transitions. The intraband contribution can be obtained from knowledge of the optical response of a single parabolic band, for instance by the usual Drude or Lindhard formulas in the normal state. The interband contribution, on the other hand, is a genuine contribution due to the QBT that cannot be captured by the theory for a single band. (We therefore also refer to it as "QBT contribution.") It also constitutes the anomalous contribution observed in Ref. [5]. We write

$$\varepsilon(\omega, \mathbf{p}) = 1 + \varepsilon^{(\mathrm{intra})}(\omega, \mathbf{p}) + \varepsilon^{(\mathrm{QBT})}(\omega, \mathbf{p}), \tag{1}$$

$$\varepsilon^{(\mathrm{intra})}(\omega, \mathbf{p}) = \varepsilon^{(\mathrm{upper})}(\omega, \mathbf{p}) + \varepsilon^{(\mathrm{lower})}(\omega, \mathbf{p}). \tag{2}$$

For nonzero E_F, one may expect only the band that is pierced by the chemical potential to contribute significantly to the response, whereas all other filled or empty bands are irrelevant. In Luttinger semimetals the QBT contribution quantifies how inaccurate this picture can be. On a more technical level, the interband contribution is conveniently incorporated by keeping the full 4×4 structure of the underlying Luttinger Hamiltonian [44] instead of projecting it onto the two-dimensional basis spaces for the upper and lower band. This conveniently incorporates interband transitions. It also accounts for the presence of Bogoliubov Fermi surfaces in certain time-reversal symmetry breaking superconducting states in QBT systems [23,45,46].

This work consists of two major parts. In the first or main part, after a review of the Luttinger Hamiltonian and optical response functions, we present the relevant formulas for the dielectric function and optical conductivity in the normal and s-wave superconducting phase and discuss their features. This presentation is intentionally left concise and does not illuminate any details on how the results were obtained. The formulas are either given in fully analytic form or as one-dimensional integrals. In order to facilitate the comparison

with experiment, results are presented in SI units, displaying the effective band mass m^* explicitly in all formula. (We employ $\hbar = k_B = 1$ throughout the article though.)

In the Supplemental Material (SM) [47] we give a self-contained derivation of the optical response of QBT Hamiltonians starting from the path integral, and then present the detailed calculation of the response functions presented in the main part. This extensive discussion of the setup also allows us to fix our notation and conventions, and set the stage for future works. Sections and equations in the SM are indicated by a prefix "S." The results for the normal state are derived in Sec. S.III and the results for the superconducting state in Sec. S.IV. We show that the QBT contribution satisfies gauge invariance in the normal state in Sec. S.III.C and derive the transverse current response in Sec. S.III.D. Algebraic conventions and matrix representations are specified in Sec. S.II. In the SM we work with Gauss units and set $2m^* = 1$.

II. LUTTINGER SEMIMETALS

We assume the band structure of the QBT point to be described by the Luttinger model. The corresponding 4×4 electronic single-particle Hamiltonian [44] reads

$$\hat{H} = \left(\alpha_1 + \frac{5}{2}\alpha_2\right)\hat{p}^2 \mathbb{1}_4 - 2\alpha_3(\hat{\mathbf{p}} \cdot \vec{J})^2 + 2(\alpha_3 - \alpha_2)\sum_{i=1}^{3} \hat{p}_i^2 J_i^2. \tag{3}$$

Here $\hat{\mathbf{p}} = -i\nabla$ is the momentum operator and $\vec{J} = (J_1, J_2, J_3)^{\mathrm{T}}$ encompasses the spin-3/2 matrices. The Luttinger parameters $\alpha_1, \alpha_2, \alpha_3$ characterize the specific details of the QBT in a given material and may be determined experimentally or from first-principle electronic band structure calculations. The number of such independent parameters is dictated by the symmetries that govern the low-energy excitations. Equation (3) captures the most general QBT Hamiltonian in the presence of time-reversal, inversion, and cubic point group symmetry. The number of independent parameters decreases upon imposing further symmetry constraints.

In order to elucidate the interplay between symmetry and band structure in the Luttinger model, we define the effective band mass m^* by

$$\frac{1}{2m^*} = |\alpha_2 + \alpha_3|, \tag{4}$$

the particle-hole asymmetry parameter by

$$x = \frac{\alpha_1}{|\alpha_2 + \alpha_3|}, \tag{5}$$

and the spatial anisotropy parameter by

$$\delta = \frac{\alpha_3 - \alpha_2}{\alpha_2 + \alpha_3} \in [-1, 1]. \tag{6}$$

The single-particle energies that follow from the Luttinger Hamiltonian then take the form

$$\begin{aligned} E_\pm(\mathbf{p}) &= \alpha_1 p^2 \pm \left[4\alpha_2^2 p^4 + 12\left(\alpha_3^2 - \alpha_2^2\right)\sum_{i<j} p_i^2 p_j^2\right]^{1/2} \\ &= \frac{1}{2m^*}\left(x p^2 \pm \left[(1-\delta)^2 p^4 + 12\delta \sum_{i<j} p_i^2 p_j^2\right]^{1/2}\right). \end{aligned} \tag{7}$$

Each eigenvalue is doubly degenerate due to time-reversal and inversion symmetry. We consider here the band inverted case which corresponds to

$$|x| < 1. \tag{8}$$

The band structure then features an upper band with positive energies E_+ and a lower band with negative energies E_- for nonzero momenta. Furthermore, for $x = 0$ the spectrum of excitations becomes particle-hole symmetric, whereas $\delta = 0$ implies a spatially isotropic band structure with

$$E_\pm(\mathbf{p}) = \frac{(x \pm 1)}{2m^*} p^2, \tag{9}$$

corresponding to an effective upper and lower band mass of

$$m^*_{\mathrm{up}} = \frac{m^*}{1+x}, \quad m^*_{\mathrm{low}} = \frac{m^*}{1-x}, \tag{10}$$

respectively. Although in a given material at hand these symmetries may not be realized exactly, it is a useful simplification to neglect x and δ in calculations as long as these parameters are small compared to unity. Therefore, unless stated otherwise we set $x = \delta = 0$ in this work, but discuss the influence of nonvanishing x and δ on the homogeneous response functions in the normal state at the end of Sec. IV B.

A particularly important role for the faithful description of experimental data by means of the Luttinger model is played by the chemical potential μ. For our investigation we allow μ to have either sign, and define the Fermi energy and Fermi momentum from its modulus according to

$$E_{\mathrm{F}} := \frac{p_{\mathrm{F}}^2}{2m^*} := |\mu|. \tag{11}$$

The condition that the low-energy physics are captured by the QBT in the band dispersion then implies that $E_{\mathrm{F}} \ll E_\kappa$, where $E_\kappa = \kappa^2/(2m^*)$ is an "ultraviolet" energy scale where either the electronic band structure deviates significantly from the quadratic dispersion for $q > \kappa$, or where other low-energy degrees of freedom such as phonons become relevant. On the other hand, the parabolic band structure may be screened by a linear band structure at low momenta that results, for instance, from adding $\hat{H}_{\mathrm{lin}} = \beta_1(\hat{\mathbf{p}} \cdot \vec{J}) + \beta_2 \sum_i p_i J_i^3$ to the Hamiltonian in Eq. (3). Such contributions arise in noncentrosymmetric materials due to asymmetric spin-orbit coupling, and their presence implies a typical "infrared" energy scale $E_{\mathrm{lin}} \sim |\beta_{1,2}| p_{\mathrm{F}}$. Consequently, the linear terms can be neglected if the chemical potential is sufficiently large so that $E_{\mathrm{lin}} \ll E_{\mathrm{F}}$ and, therefore, the relevant excitations at the Fermi level are dominated by the quadratic terms. Consequently, in the

following the limit $\mu \to 0$ needs to be understood within the Luttinger model, meaning that the Fermi level is close enough to the QBT point so that $\mu \approx 0$ is a good approximation, but the chemical potential is still large enough so that linearly dispersing terms at even lower energies (if present) are irrelevant.

III. OPTICAL RESPONSE FUNCTIONS

The electrodynamic properties of solids in the linear response regime are encoded in the dielectric tensor ε_{ij} relating electric displacement field $\vec{D}$ and electric field $\vec{E}$ according to [48–50]

$$D_i(\omega, \mathbf{p}) = \epsilon_0 \varepsilon_{ij}(\omega, \mathbf{p}) E_j(\omega, \mathbf{p}). \tag{12}$$

Here ϵ_0 is the vacuum permittivity, ω and $\mathbf{p}$ constitute (angular) frequency and momentum of the incident electromagnetic field, and we have defined ε_{ij} to be a dimensionless quantity. Throughout this work we use the Einstein sum convention that we sum over repeated indices. In the following we consider nonmagnetic materials with permeability equal to 1. The linear response is then equivalently expressed in terms of the conductivity σ_{ij} given by

$$\sigma_{ij}(\omega, \mathbf{p}) = i\omega\epsilon_0[\delta_{ij} - \varepsilon_{ij}(\omega, \mathbf{p})], \tag{13}$$

which relates the internal current density $\vec{j}_{\text{int}}$ and electric field according to

$$j_{\text{int},i}(\omega, \mathbf{p}) = \sigma_{ij}(\omega, \mathbf{p}) E_j(\omega, \mathbf{p}). \tag{14}$$

In a spatially isotropic medium, the tensorial response functions for nonzero $\mathbf{p}$ can be decomposed into longitudinal (L) and transverse (T) components according to

$$\sigma_{ij}(\omega, \mathbf{p}) = \sigma_{\text{L}}(\omega, p)\frac{p_i p_j}{p^2} + \sigma_{\text{T}}(\omega, p)\left(\delta_{ij} - \frac{p_i p_j}{p^2}\right). \tag{15}$$

Crucially, a longitudinal (transverse) electromagnetic probe field can only induce a longitudinal (transverse) response, i.e.,

$$\vec{j}_{\text{int,L}}(\omega, \mathbf{p}) = \sigma_{\text{L}}(\omega, p)\vec{E}_{\text{L}}(\omega, \mathbf{p}), \tag{16}$$

$$\vec{j}_{\text{int,T}}(\omega, \mathbf{p}) = \sigma_{\text{T}}(\omega, p)\vec{E}_{\text{T}}(\omega, \mathbf{p}), \tag{17}$$

with the usual definition of the longitudinal and transverse parts of the vector fields. Equation (13) implies

$$\sigma_{\text{L}}(\omega, p) = i\omega\epsilon_0[1 - \varepsilon_{\text{L}}(\omega, p)], \tag{18}$$

$$\sigma_{\text{T}}(\omega, p) = i\omega\epsilon_0[1 - \varepsilon_{\text{T}}(\omega, p)]. \tag{19}$$

The advantage of studying $\sigma_{\text{L,T}}(\omega, p)$ over $\sigma_{ij}(\omega, \mathbf{p})$ lies in the fact that the L and T components are scalar functions of $p = |\mathbf{p}|$, and so the limit $p \to 0$ is defined unambiguously.

The experiments we attempt to quantify with our analysis are such that the spatial inhomogeneity of the external probe fields is irrelevant so that setting $\mathbf{p} = 0$ is a valid approximation. In this limit, the distinction between L and T components is meaningless and Eq. (14) provides a definition of $\sigma_{ij}(\omega, \mathbf{0})$ that does not require referencing to an external momentum. The tensorial character of this quantity is necessarily trivial and so

$$\sigma_{ij}(\omega, \mathbf{0}) = \sigma(\omega)\delta_{ij}, \tag{20}$$

which defines the homogeneous conductivity $\sigma(\omega)$. This quantity also coincides with the $\mathbf{p} \to \mathbf{0}$ limit of the L and T contributions when the limit is taken for $\omega > 0$, as generally the limits $p \to 0$ and $\omega \to 0$ do not commute. In fact, although any spatial dependence of the electric field is unimportant, in practice it will not be strictly zero. We can then perform the limit $\mathbf{p} \to 0$ in Eq. (15) explicitly by assuming (without loss of generality) that the strongest spatial inhomogeneity of $\mathbf{p}$ is in the z direction, hence $\mathbf{p} \approx (0, 0, p)^{\text{T}}$. Then, by computing the individual components $\sigma_{ij}(\omega, \mathbf{p})$ in the limit $p \to 0$ and comparing to Eq. (20), we deduce that

$$\varepsilon(\omega) = \varepsilon_{\text{L}}(\omega, 0) = \varepsilon_{\text{T}}(\omega, 0), \tag{21}$$

$$\sigma(\omega) = \sigma_{\text{L}}(\omega, 0) = \sigma_{\text{T}}(\omega, 0). \tag{22}$$

Equations (21) and (22) allow us to conveniently discuss the optical response of materials in terms of a single frequency-dependent function.

In order to facilitate the comparison with experiment we employ SI units here with $\epsilon_0 = 8.854 \times 10^{-12}\ \text{F m}^{-1}$ and electric charge $e = 1.602 \times 10^{-19}$ C. For computing the response functions from the underlying microscopic model, as it is presented in the SM [47], we conveniently use Gauss units. The corresponding electric charge in Gauss units will be denoted by an overbar, and is given by $\bar{e} = 1.519 \times 10^{-14}\ \text{m}^{3/2}\,\text{kg}^{1/2}\,\text{s}^{-1}$. Both quantities are related by

$$\bar{e}^2 = \frac{e^2}{4\pi\epsilon_0}. \tag{23}$$

Furthermore, the dielectric function and conductivity in Gauss units, denoted as $\bar{\varepsilon}$ and $\bar{\sigma}$ with an overbar, are defined from $\vec{D}(\omega, \mathbf{p}) = \bar{\varepsilon}(\omega, \mathbf{p})\vec{E}(\omega, \mathbf{p})$ and $\vec{j}_{\text{int}}(\omega, \mathbf{p}) = \bar{\sigma}(\omega, \mathbf{p})\vec{E}(\omega, \mathbf{p})$. They are mutually related by $\bar{\sigma}(\omega, \mathbf{p}) = \frac{i\omega}{4\pi}[1 - \bar{\varepsilon}(\omega, \mathbf{p})]$, and are obtained from the response function in SI units by means of

$$\bar{\varepsilon}(\omega, \mathbf{p}) = \varepsilon(\omega, \mathbf{p}), \tag{24}$$

$$\bar{\sigma}(\omega, \mathbf{p}) = \frac{1}{4\pi\epsilon_0}\sigma(\omega, \mathbf{p}), \tag{25}$$

with the charge translated according to Eq. (23).

Our approach to computing the optical response lies in a field theoretic determination of the density-density response function $-\chi(\omega, p)$ and current-current response function $-K_{ij}(\omega, \mathbf{p})$ within RPA. We refer to the SM [47] for their definition, and limit ourselves here to a brief discussion of their key properties. We first note that gauge invariance implies

$$\omega^2\chi(\omega, p) = -p^2 K_{\text{L}}(\omega, p). \tag{26}$$

The L component of the dielectric function is given by

$$\varepsilon_{\text{L}}(\omega, p) = 1 + 4\pi\frac{\chi(\omega, p)}{p^2}, \tag{27}$$

and the conductivity reads

$$\sigma_{ij}(\omega, \mathbf{p}) = -\frac{4\pi\epsilon_0}{i\omega} K_{ij}(\omega, \mathbf{p}). \tag{28}$$

Equation (26) guarantees that the L components satisfy $\sigma_{\mathrm{L}} = i\omega\epsilon_0(1 - \varepsilon_{\mathrm{L}})$. Furthermore, it implies that $\chi(\omega, 0) = 0$ for $\omega > 0$. For small momenta we may then expand the density response in power of p and obtain

$$\chi(\omega, p) = Z(\omega)p^2 + O(p^4). \tag{29}$$

Consequently, in the limit $\mathbf{p} = 0$ the dielectric function is given by

$$\varepsilon(\omega) = 1 + 4\pi Z(\omega), \tag{30}$$

and we have $\sigma(\omega) = -i\omega 4\pi\epsilon_0 Z(\omega)$ for the conductivity.

The function $K_{ij}(\omega, \mathbf{p})$ is useful for studying several important conceptual aspects of the optical response of media [51]. First note that gauge invariance through Eq. (26) implies $K_{\mathrm{L}}(0, p) = 0$. Hence the static response (meaning $\omega = 0$) is purely transverse. On a technical level, the absence of the static L component requires a perfect cancellation between the diamagnetic (d) and paramagnetic (p) contributions to the current-current response. Referring to the SM [47] for details of their definition, we note here that the response function is naturally split into the diamagnetic and paramagnetic contributions according to

$$K_{ij}(\omega, \mathbf{p}) = K_{ij}^{(\mathrm{d})}(\omega, \mathbf{p}) + K_{ij}^{(\mathrm{p})}(\omega, \mathbf{p}). \tag{31}$$

Whereas the perfect cancellation is also valid for the static T component in the normal state, this situation is fundamentally altered in the superconducting state. Intuitively, the diamagnetic contribution comes from all electrons of the system, whereas only electrons on the Fermi surface contribute to the paramagnetic term. Since electron excitations at the Fermi surface are gapped (hence only thermally populated) in a superconductor, the diamagnetic term then dominates over the paramagnetic one. In this context, the superfluid density n_{s} is defined according to

$$\lim_{p\to 0} K_{\mathrm{T}}(0, p) = \frac{e^2 n_{\mathrm{s}}}{4\pi\epsilon_0 m^*}. \tag{32}$$

Clearly we have $n_{\mathrm{s}} = 0$ in the normal state. For a clean single-band superconductor in the mean-field approximation, we find that the paramagnetic contribution vanishes completely at zero temperature, and the transverse response is entirely given by the diamagnetic term $K_{\mathrm{T}}^{(\mathrm{d})}(\omega, p) = \frac{e^2 n}{4\pi\epsilon_0 m^*}$, and so the superfluid density agrees with the electron density: $n_{\mathrm{s}} = n$. In a more realistic setup, considering interaction and impurity effects, we generally have $n_{\mathrm{s}} < n$ even at zero temperature.

IV. NORMAL STATE RESPONSE

We begin our analysis of optical response in Luttinger semimetals by considering systems in the normal state. Unless explicitly stated we consider the particle-hole and rotationally symmetric case with $x = \delta = 0$, which encompasses the key qualitative features of the optical response within the Luttinger model as long as these parameters are small compared to unity. The formulas presented here are derived in Sec. S.III of the SM [47].

A. Scales and limits

The optical response in the normal state is determined by the frequency and momentum of the probe field ω and p, and the thermodynamic parameters μ and T. The density of charge carriers within RPA reads

$$n = 2\int_{\mathbf{q}} \left[n_{\mathrm{F}}\left(\frac{q^2}{2m^*} - \mu\right) + n_{\mathrm{F}}\left(\frac{q^2}{2m^*} + \mu\right)\right], \tag{33}$$

where we denote $\int_{\mathbf{q}} = \int \frac{d^3q}{(2\pi)^3}$ and $n_{\mathrm{F}}(E) = (e^{E/T} + 1)^{-1}$. At zero temperature we obtain

$$n_0 := \frac{p_{\mathrm{F}}^3}{3\pi^2} = \frac{(2m^*|\mu|)^{3/2}}{3\pi^2}. \tag{34}$$

This coincides with the density of carriers of a single parabolic band at zero temperature since fluctuation effects between electrons in distinct bands are suppressed in our mean-field approximation.

In the following we consider two ways of taking the low-momentum limit $p^2/(2m^*\omega) \to 0$, which is typically well satisfied for spectroscopic experiments. The first approach, which we refer to as the *homogeneous limit*, corresponds to taking the limit for a fixed ratio of ω/μ. This basically corresponds to setting $p = 0$ in the response functions. Importantly, in the homogeneous limit, longitudinal and transverse response coincide. The second way to perform the limit, which we refer to as *quasistatic limit*, corresponds to keeping the ratio ω/vp fixed, where

$$v := \frac{p_{\mathrm{F}}}{m^*} = \sqrt{\frac{2|\mu|}{m^*}} \tag{35}$$

is the Fermi velocity. Clearly $\frac{p^2}{2m^*\omega} \to 0$ while $\frac{\omega}{vp} < \infty$ implies that $\omega \ll \mu$. The dominance of the chemical potential over all other scales, on the other hand, is a common scenario in solid state systems and thus clearly deserves consideration here. If in addition $\omega/vp \ll 1$ we are in a regime such that

$$\frac{p^2}{2m^*} \ll \omega \ll vp. \tag{36}$$

These inequalities are often taken as the definition of the quasistatic limit [49], so our definition is slightly more generous. We summarize the setup in Fig. 2.

B. Homogeneous limit

The intraband contribution from the upper and lower bands in the clean limit takes the usual form

$$\varepsilon^{(\mathrm{intra})}(\omega) = -\frac{\omega_{\mathrm{p}}^2}{\omega(\omega + i0)}, \tag{37}$$

$$\sigma^{(\mathrm{intra})}(\omega) = -\frac{\epsilon_0\omega_{\mathrm{p}}^2}{i(\omega + i0)}, \tag{38}$$

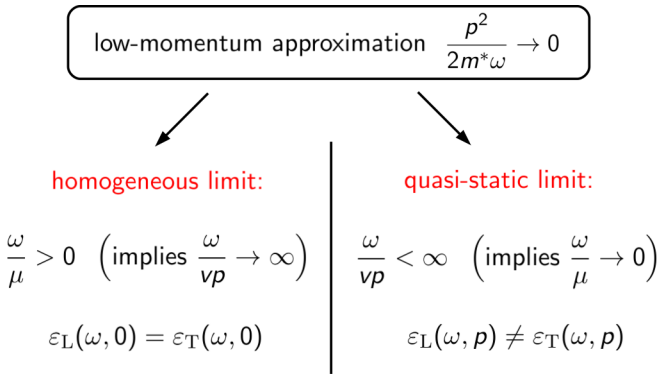

FIG. 2. The low-momentum regime with $p^2/(2m^*) \ll \omega$ naturally decomposes into two sectors depending on whether the product vp with Fermi velocity $v \propto \sqrt{E_{\rm F}}$ is dominating or irrelevant compared to the remaining energy scales such as ω or T. For $vp \ll \omega$, which amounts to setting $p = 0$ in practice, we obtain the homogeneous limit, where L and T response coincide. For $vp \gtrsim \omega$, on the other hand, frequencies are necessarily small compared to μ and hence this regime is labeled the quasistatic limit. The inherent momentum dependence of the response then implies that L and T contributions differ.

with the plasma frequency $\omega_{\rm p}$ defined from the carrier density n according to

$$\omega_{\rm p}^2 = \frac{ne^2}{\epsilon_0 m^*}. \tag{39}$$

The individual contributions from the upper and lower bands to the conductivity are given by

$$\varepsilon^{(\rm upper)}(\omega) = -\frac{2e^2}{\epsilon_0 m^*}\frac{1}{\omega^2}\int_{\mathbf{q}} n_{\rm F}\left(\frac{q^2}{2m^*} - \mu\right), \tag{40}$$

$$\varepsilon^{(\rm lower)}(\omega) = -\frac{2e^2}{\epsilon_0 m^*}\frac{1}{\omega^2}\int_{\mathbf{q}} n_{\rm F}\left(\frac{q^2}{2m^*} + \mu\right). \tag{41}$$

The effect of nonmagnetic impurities can be included in Eqs. (37) and (38) by a shift $\omega \to \omega + i/\tau$ with scattering time τ, or scattering rate $\Gamma = \tau^{-1}$. Assuming for simplicity that the scattering rates for the upper and lower band are equal, we obtain

$$\varepsilon^{(\rm intra)}(\omega) = -\frac{\omega_{\rm p}^2}{\omega(\omega + i/\tau)}, \tag{42}$$

$$\sigma^{(\rm intra)}(\omega) = \frac{\epsilon_0 \omega_{\rm p}^2 \tau}{1 - i\omega\tau}. \tag{43}$$

For large scattering rate, the conductivity is approximately real and frequency independent. For small scattering rate $\tau^{-1} \to 0$, on the other hand, Eq. (38) implies

$$\sigma_1^{(\rm intra)}(\omega) = \frac{\pi}{2}\frac{ne^2}{m^*}\delta(\omega), \tag{44}$$

$$\sigma_2^{(\rm intra)}(\omega) = \frac{ne^2}{m^*\omega} \tag{45}$$

for the real and imaginary parts. The δ-function in $\sigma_1(\omega)$ is restricted to non-negative frequencies, hence the normalization with $\pi/2$.

The interband or QBT contribution to the dielectric function in the clean limit is given by [39]

$$\varepsilon^{(\rm QBT)}(\omega) = \frac{e^2}{4\pi\epsilon_0}\sqrt{\frac{m^*}{\omega}}(1+i) - \frac{2e^2}{\epsilon_0 m^*}\int_{\mathbf{q}} \frac{n_{\rm F}\left(\frac{q^2}{2m^*} - \mu\right) + n_{\rm F}\left(\frac{q^2}{2m^*} + \mu\right)}{-(\omega + i0)^2 + q^4/(m^*)^2}. \tag{46}$$

Here the first contribution is of particular significance. Its peculiar form originates from the appearance of the square root of $i\omega$ after analytic continuation from Matsubara frequencies $p_0, ip_0 \to \omega + i0$, according to

$$\frac{1}{\sqrt{p_0}} \to \frac{1}{\sqrt{-i\omega}} = \frac{1}{\sqrt{2\omega}}(1+i). \tag{47}$$

In the limit $\mu, T \to 0$, only the first line of Eq. (46) contributes to the response, and we obtain a $1/\sqrt{\omega}$-divergent low-energy response according to

$$\lim_{\mu,T\to 0} \varepsilon^{(\rm QBT)}(\omega) = \frac{e^2}{4\pi\epsilon_0}\sqrt{\frac{m^*}{\omega}}(1+i). \tag{48}$$

Since the intraband contribution from the upper and lower bands vanishes in this limit, the optical response is then entirely dominated by the interband transitions, and thus genuinely different from a single band system.

For general μ and T, the imaginary part of Eq. (46) can be computed analytically and reads

$$\varepsilon_2^{(\rm QBT)}(\omega) = \frac{e^2}{4\pi\epsilon_0}\sqrt{\frac{m^*}{\omega}}\left[1 - n_{\rm F}\left(\frac{\omega}{2} - \mu\right) - n_{\rm F}\left(\frac{\omega}{2} + \mu\right)\right]. \tag{49}$$

In particular, at zero temperature we arrive at

$$\varepsilon_2^{(\rm QBT)}(\omega) = \frac{e^2}{4\pi\epsilon_0}\sqrt{\frac{m^*}{\omega}}\theta(\omega - 2E_{\rm F}). \tag{50}$$

In order to compute the real part of Eq. (46) for nonzero temperatures, the integral can be evaluated for a small finite value of $i0$ or in terms of the principal value. At zero temperature we have

$$\varepsilon_1^{(\rm QBT)}(\omega) = \frac{e^2}{4\pi\epsilon_0}\sqrt{\frac{m^*}{\omega}}\left[1 - \frac{2}{\pi}\arctan\left(\sqrt{\frac{2E_{\rm F}}{\omega}}\right) - \frac{1}{\pi}\ln\left(\frac{|1 - \sqrt{\omega/(2E_{\rm F})}|}{1 + \sqrt{\omega/(2E_{\rm F})}}\right)\right]. \tag{51}$$

In the limit $\omega \to 0$ we are left with a real response given by

$$\varepsilon^{(\rm QBT)}(0) = \frac{e^2}{2\pi^2\epsilon_0}\sqrt{\frac{2m^*}{E_{\rm F}}}. \tag{52}$$

We observe that a nonzero Fermi energy regularizes the $1/\sqrt{\omega}$ divergence of both the real and imaginary parts of the low-frequency response. We display the temperature dependence of the QBT contribution in Fig. 3.

In the spatially anisotropic case with $\delta \neq 0$ (while still keeping particle-hole symmetry so that $x = 0$), the intraband

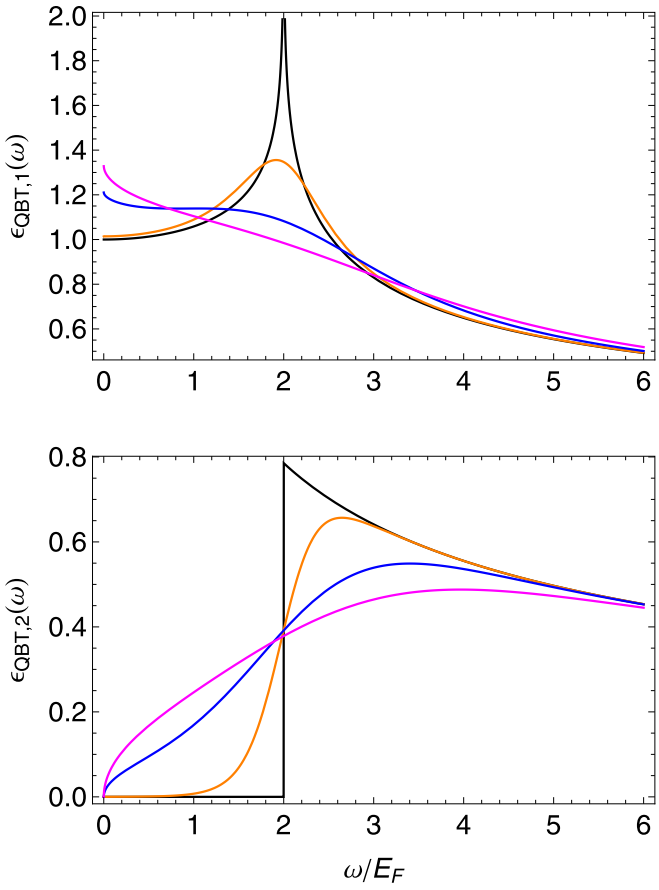

FIG. 3. QBT contribution to the homogeneous dielectric function $\varepsilon(\omega)$. We show the real and imaginary part in the upper and lower plot, respectively, as a function of ω/E_{F}. Here we normalize the expressions by the zero temperature limit $\varepsilon(0) = \frac{e^2}{2\pi^2\epsilon_0}\sqrt{2m^*/E_{\mathrm{F}}}$. The distinct curves (from bottom to top along the zero frequency axis) correspond to T/E_{F} values of 0 (black), 0.1 (orange), 0.3 (blue), and 0.5 (magenta). At zero temperature we observe singular behavior at $\omega = 2E_{\mathrm{F}}$, which extends to an anomalously large, $1/\sqrt{\omega}$-divergent contribution to both the real and imaginary parts of the optical response as $E_{\mathrm{F}} \to 0$. At nonzero temperature the functions remain regular.

and interband contributions to the response functions factorize into the isotropic formula and a δ-dependent prefactor. In particular, this prefactor is identical for the individual terms, and so we have an overall factorization according to

$$\sigma(\omega) = \frac{\lambda(\delta)}{\sqrt{1-\delta^2}}\sigma(\omega)|_{\delta=0}. \tag{53}$$

The factorization also holds for nonzero temperatures. Here $\lambda(\delta)$ is a regular function for all values of δ and can be computed numerically to arbitrary precision in terms of the two-dimensional angular integral given in Eq. (S.164) in the SM [47]. For all practical purposes the quadratic approximation

$$\lambda(\delta) = 1 - \frac{1}{10}\delta + \frac{229}{280}\delta^2 + O(\delta^3) \tag{54}$$

should be sufficient, which captures the exact function with 10% accuracy. Equation (53) then implies a divergent response in the strongly anisotropic limits $\delta \to \pm 1$, resulting in an increase of conductivity. We display $\lambda(\delta)$ together with the quadratic approximation in Fig. 4.

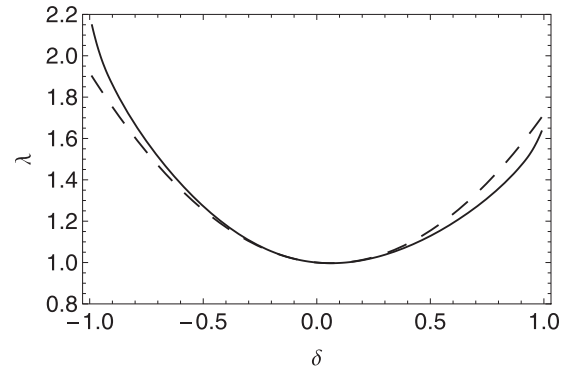

FIG. 4. The homogeneous optical response for nonvanishing spatial anisotropy δ gets renormalized by a prefactor $\lambda(\delta)/\sqrt{1-\delta^2}$ that diverges for strong anisotropy. This statement is true for both the intraband and interband contributions, at both zero and nonzero temperature, for $x = 0$. For $\delta = 0$ we have, of course, $\lambda(0) = 1$. The solid line shows the function $\lambda(\delta)$ computed from the two-dimensional integral in Eq. (S.164) in the SM [47], whereas the dashed line corresponds to the expansion around $\delta = 0$ to quadratic order from Eq. (54). The latter should be sufficient for all practical purposes.

In the particle-hole asymmetric case with $x \neq 0$ (while maintaining spatial isotropy $\delta = 0$ for simplicity), the intraband contributions are obtained by replacing the mass m^* with the effective band masses from Eq. (10) and thus read

$$\varepsilon^{(\mathrm{upper})}(\omega) = -\frac{2e^2}{\epsilon_0 m^*_{\mathrm{up}}}\frac{1}{\omega^2}\int_{\mathbf{q}} n_{\mathrm{F}}\left(\frac{q^2}{2m^*_{\mathrm{up}}} - \mu\right), \tag{55}$$

$$\varepsilon^{(\mathrm{lower})}(\omega) = -\frac{2e^2}{\epsilon_0 m^*_{\mathrm{low}}}\frac{1}{\omega^2}\int_{\mathbf{q}} n_{\mathrm{F}}\left(\frac{q^2}{2m^*_{\mathrm{low}}} + \mu\right). \tag{56}$$

The corresponding QBT contribution in the absence of particle-hole symmetry is given by

$$\varepsilon^{(\mathrm{QBT})}(\omega) = \frac{e^2}{4\pi\epsilon_0}\sqrt{\frac{m^*}{\omega}}(1+i) - \frac{2e^2}{\epsilon_0 m^*}\int_{\mathbf{q}} \frac{n_{\mathrm{F}}\left(\frac{q^2}{2m^*_{\mathrm{up}}} - \mu\right) + n_{\mathrm{F}}\left(\frac{q^2}{2m^*_{\mathrm{low}}} + \mu\right)}{-(\omega+i0)^2 + q^4/(m^*)^2}, \tag{57}$$

see our discussion at the end of Sec. S.III.A of the SM [47]. Therein we also describe how $x \neq 0$ can be implemented easily when needed, which is necessary for studying the optical response of materials with sizable x, while still keeping $|x| < 1$ in order to have an inverted band structure. For the half-Heusler material YPtBi, however, $x \simeq 0.17$ is estimated to be small [6,27]. Furthermore, x is an irrelevant parameter in the sense of the renormalization group so that $x \to 0$ for $\mu = 0$ and very low frequencies [18,22]. Hence for the rest of the paper we assume $x = 0$, which additionally implies an appealingly symmetric structure of the results.

C. Quasistatic limit

We now discuss the intraband and interband contributions in the quasistatic limit, where longitudinal and transverse components differ. We begin with the zero temperature case as it allows us to give analytical expressions for the response functions. We assume $x = \delta = 0$. The intraband contributions to the longitudinal and transverse response functions in the limit $p^2/(2m^*\omega) \to 0$ with ω/vp held fixed read

$$\varepsilon_{\rm L}^{(\rm intra)}(\omega, p) = \frac{n_0 e^2}{\epsilon_0 m^*}\frac{3}{v^2p^2}\left[1 - \frac{\omega}{2vp}\ln\left(\frac{\omega + vp + i0}{\omega - vp + i0}\right)\right], \tag{58}$$

$$\varepsilon_{\rm T}^{(\rm intra)}(\omega, p) = -\frac{n_0 e^2}{\epsilon_0 m^*}\frac{3}{2v^2p^2}\left\{1 + \frac{vp}{2\omega}\left[1 - \left(\frac{\omega}{vp}\right)^2\right] \times \ln\left(\frac{\omega + vp + i0}{\omega - vp + i0}\right)\right\}. \tag{59}$$

Here the logarithm for nonzero $0 \neq r \in \mathbb{R}$ is defined as

$$\ln(r \pm i0) = \begin{cases} \ln r & (r > 0), \\ \ln(-r) \pm i\pi & (r < 0). \end{cases} \tag{60}$$

Note that the longitudinal contribution is logarithmically divergent for $\omega = vp$, whereas the transverse contributions remains finite for this frequency. We plot the functions, together with the finite temperature results presented below, in Fig. 5.

It is instructive to expand the response as a function of ω/vp in the asymptotic regimes. For $\omega \ll vp$ we obtain

$$\varepsilon_{\rm L}^{(\rm intra)}(\omega, p) = \frac{n_0 e^2}{\epsilon_0 m^*}\frac{3}{p^2v^2}\left[1 + \frac{\pi}{2}\frac{i\omega}{vp} - \left(\frac{\omega}{vp}\right)^2\right], \tag{61}$$

$$\varepsilon_{\rm T}^{(\rm intra)}(\omega, p) = \frac{n_0 e^2}{\epsilon_0 m^*}\frac{3\pi}{4\omega^2}\frac{i\omega}{vp}\left[1 + \frac{4}{\pi}\frac{i\omega}{vp} - \left(\frac{\omega}{vp}\right)^2 + \cdots\right]. \tag{62}$$

We observe that the leading L contribution is real, whereas the T contribution is predominantly imaginary. Furthermore, the L component is subleading compared to the T component, as it is suppressed by an additional power of ω/vp. The response functions in the quasistatic limit can also be expanded for $vp/\omega \ll 1$, which yields

$$\varepsilon_{\rm L}^{(\rm intra)}(\omega, p) = -\frac{n_0 e^2}{\epsilon_0 m^*}\frac{1}{\omega^2}\left[1 + \frac{3}{5}\left(\frac{vp}{\omega}\right)^2 + \cdots\right], \tag{63}$$

$$\varepsilon_{\rm T}^{(\rm intra)}(\omega, p) = -\frac{n_0 e^2}{\epsilon_0 m^*}\frac{1}{\omega^2}\left[1 + \frac{1}{5}\left(\frac{vp}{\omega}\right)^2 + \cdots\right]. \tag{64}$$

We observe to recover the homogeneous result in the limit $vp/\omega \to 0$.

The interband or QBT contributions at zero temperature in the quasistatic limit read

$$\varepsilon_{\rm L}^{(\rm QBT)}(\omega, p) = \frac{e^2}{4\pi^2\epsilon_0}\sqrt{\frac{2m^*}{E_{\rm F}}}\left\{1 + \frac{3}{2}\left(\frac{\omega}{vp}\right)^2 + \frac{3\omega}{4vp}\left[1 - \left(\frac{\omega}{vp}\right)^2\right]\ln\left(\frac{\omega + vp + i0}{\omega - vp + i0}\right)\right\}, \tag{65}$$

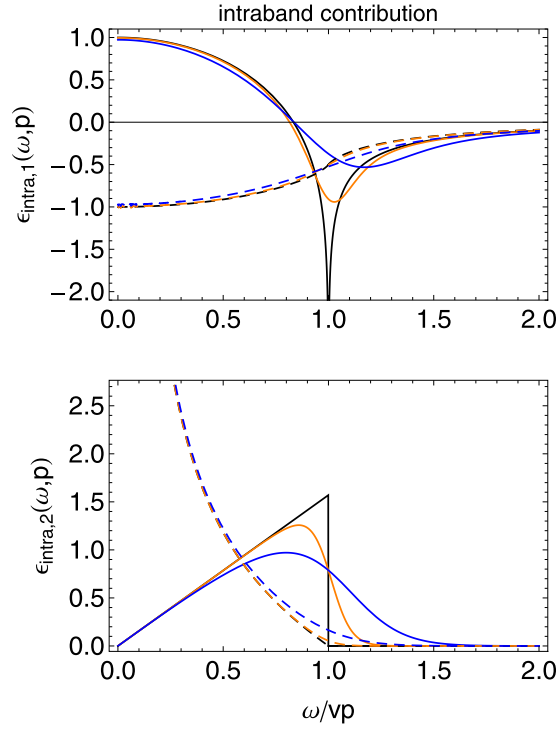

FIG. 5. Intraband contributions to the dielectric tensor in the quasistatic limit as a function of ω/vp. Results are plotted in units of $\frac{n_0e^2}{\epsilon_0 m^*}\frac{3}{p^2v^2}$, the solid lines constitute the longitudinal response, the dashed lines the transverse response. The zero temperature results, shown in black, display singular behavior at $\omega = vp$. In particular, the real longitudinal component diverges logarithmically at this point. At nonzero temperature the functions are regular, shown here for $T/E_{\rm F} = 0.1$ (orange) and $T/E_{\rm F} = 0.3$ (blue). We observe the leading contribution at small frequencies to be imaginary and transverse. For large $\omega/vp \gg 1$, longitudinal and transverse response converge to the homogeneous limit.

$$\varepsilon_{\rm T}^{(\rm QBT)}(\omega, p) = \frac{5e^2}{8\pi^2\varepsilon_0}\sqrt{\frac{2m^*}{E_{\rm F}}}\left[1 + \frac{3}{4}\left(\frac{\omega}{vp}\right)^{-2}\right] \times \left\{1 - \frac{3}{10}\left(\frac{\omega}{vp}\right)^2 - \frac{3\omega}{20vp}\left[1 - \left(\frac{\omega}{vp}\right)^2\right]\ln\left(\frac{\omega + vp + i0}{\omega - vp + i0}\right)\right\}. \tag{66}$$

The corresponding real and imaginary parts are shown in Fig. 6, together with the finite temperature results. Both longitudinal and transverse response, although nonanalytic at $\omega = vp$, remain finite at this frequency. Expanding the QBT contribution in powers of ω/vp we obtain

$$\varepsilon_{\rm L}^{(\rm QBT)}(\omega, p) = \frac{e^2}{4\pi^2\epsilon_0}\sqrt{\frac{2m^*}{E_{\rm F}}}\left[1 - \frac{3\pi}{4}\frac{i\omega}{vp} + 3\left(\frac{\omega}{vp}\right)^2 + \cdots\right], \tag{67}$$

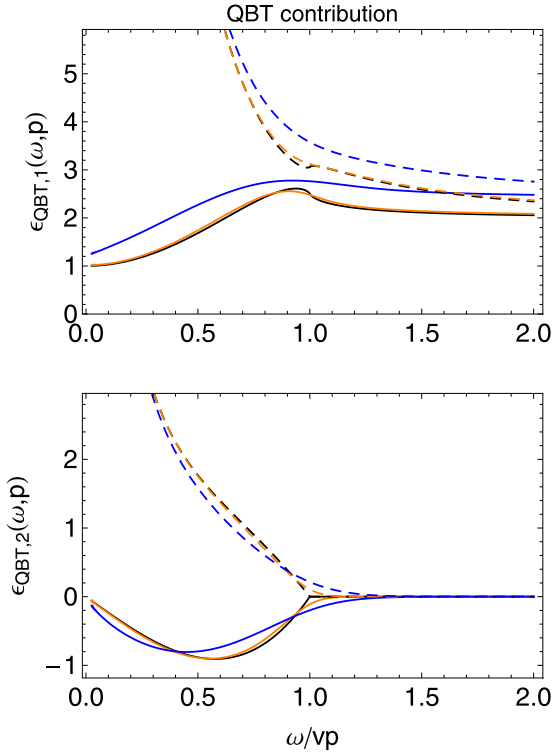

FIG. 6. QBT contribution to the dielectric tensor in the quasistatic limit as a function of ω/vp. Curves are normalized by $\frac{e^2}{4\pi^2\epsilon_0}\sqrt{2m^*/E_F}$, and longitudinal (solid lines) and transverse (dashed lines) contributions are shown for $T/E_F = 0$ (black), $T/E_F = 0.1$ (orange), and $T/E_F = 0.3$ (blue). The interband contributions remain finite at $\omega = vp$, although showing nonanalytic behavior at zero temperature. For large ω/vp we recover the large additive contribution to the real part of $\varepsilon(\omega)$. For small ω/vp, the longitudinal contribution settles at a real value which is half the homogeneous limit. The transverse component diverges in both the real and imaginary parts with the real part being most dominant. As a result, the limit $\omega/vp \to 0$ of $\varepsilon_{L,T}(\omega, p)$ is fully dominated by the QBT contribution, see the discussion in the main text.

$$\varepsilon_T^{(QBT)}(\omega, p) = \frac{15e^2}{32\pi^2\epsilon_0}\sqrt{\frac{2m^*}{E_F}}\left(\frac{\omega}{vp}\right)^{-2} \times \left[1 + \frac{3\pi i}{20}\frac{\omega}{vp} + \frac{11}{15}\left(\frac{\omega}{vp}\right)^2 + \cdots\right]. \quad (68)$$

In contrast to the intraband response, both leading contributions are real. Furthermore, as $\omega/vp \to 0$ we observe that the longitudinal response becomes frequency independent and settles at half the homogeneous value for $\omega \ll \mu$ given by $\varepsilon^{(QBT)}(0) = \frac{e^2}{2\pi^2\epsilon_0}\sqrt{\frac{2m^*}{E_F}}$. In contrast, the transverse contribution is divergent as $\omega/vp \to 0$. The quasistatic limit expressions for $vp/\omega \ll 1$ read

$$\varepsilon_L^{(QBT)}(\omega, p) = \frac{e^2}{2\pi^2\epsilon_0}\sqrt{\frac{2m^*}{E_F}}\left[1 + \frac{1}{10}\left(\frac{vp}{\omega}\right)^2 + \cdots\right], \quad (69)$$

$$\varepsilon_T^{(QBT)}(\omega, p) = \frac{e^2}{2\pi^2\epsilon_0}\sqrt{\frac{2m^*}{E_F}}\left[1 + \frac{7}{10}\left(\frac{vp}{\omega}\right)^2 + \cdots\right]. \quad (70)$$

In particular, for $vp/\omega \to 0$ we obtain the homogeneous result for $\omega \ll \mu$, whereas the nontrivial frequency dependence of the homogeneous QBT contribution is lost in the quasistatic limit at zero temperature.

The very distinct behavior of the intraband and interband contributions as a function of ω/vp is striking. For large ω/vp, and so in the homogeneous limit, the QBT contribution is frequency independent and amounts to the constant anomalous contribution adding to the real part of $\varepsilon(\omega)$. For small ω/vp, on the other hand, the intraband contributions are suppressed by powers of ω/vp or $(\omega/vp)^2$. The QBT contributions, on the other hand, are real and remain constant (longitudinal component) or diverge like $(\omega/vp)^{-2}$ (transverse component). Hence the quasistatic limit is entirely dominated by the interband transitions and so genuinely different from systems with a single parabolic band.

At nonzero temperature the intraband contributions to the longitudinal and transverse response in the quasistatic limit are given by

$$\varepsilon_L^{(intra)}(\omega, p) = \frac{2e^2}{\epsilon_0 m^*}\int_{\mathbf{q}} \frac{n_F\left(\frac{q^2}{2m^*} - \mu\right) + n_F\left(\frac{q^2}{2m^*} + \mu\right)}{-(\omega + i0)^2 + q^2p^2/(m^*)^2}, \quad (71)$$

$$\varepsilon_T^{(intra)}(\omega, p) = -\frac{e^2}{\epsilon_0\omega}\int_{\mathbf{q}} \frac{n_F\left(\frac{q^2}{2m^*} - \mu\right) + n_F\left(\frac{q^2}{2m^*} + \mu\right)}{qp} \times \ln\left(\frac{\omega + qp^* + i0}{\omega - qp^* + i0}\right), \quad (72)$$

with $p^* = p/m^*$. We observe that a finite temperature regularizes the logarithmic divergence of the longitudinal contribution at $\omega = vp$. The temperature dependence of the transverse response is weak. The QBT contributions at finite temperature read

$$\varepsilon_L^{(QBT)}(\omega, p) = \varepsilon^{(QBT)}(\omega) + \frac{e^2m^*}{\epsilon_0}\int_{\mathbf{q}} \frac{n_F\left(\frac{q^2}{2m^*} - \mu\right) + n_F\left(\frac{q^2}{2m^*} + \mu\right)}{q^4} \times \left\{1 - 6\left(\frac{\omega}{qp^*}\right)^2 - \frac{3\omega}{2qp^*}\left[1 - 2\left(\frac{\omega}{qp^*}\right)^2\right]\ln\left(\frac{\omega + qp^* + i0}{\omega - qp^* + i0}\right)\right\} \quad (73)$$

and

$$\varepsilon_T^{(QBT)}(\omega, p) = \varepsilon^{(QBT)}(\omega) + \frac{15e^2m^*}{8\varepsilon_0}\int_{\mathbf{q}} \frac{n_F\left(\frac{q^2}{2m^*} - \mu\right) + n_F\left(\frac{q^2}{2m^*} + \mu\right)}{q^4} \times \left\{\left(\frac{\omega}{qp^*}\right)^{-2} + \frac{1}{3} + \frac{8}{5}\left(\frac{\omega}{qp^*}\right)^2 + \frac{\omega}{10qp^*}\left[1 - 8\left(\frac{\omega}{qp^*}\right)^2\right]\log\left(\frac{\omega + qp^* + i0}{\omega - qp^* + i0}\right)\right\}. \quad (74)$$

Here $\varepsilon^{(\mathrm{QBT})}(\omega)$ is the homogeneous contribution from Eq. (46). For nonzero temperature this term can have a residual (nonuniversal) dependence on ω/E_F. For this note that for a generic value of $\omega/vp \sim 1$, we have $\omega/E_\mathrm{F} \sim p^2/(2m^*\omega)$. Hence, although $\omega/E_\mathrm{F} \to 0$ in the strict quasistatic limit, a finite value of p implies a nonzero value of ω/E_F. This small value of ω/E_F does not affect the zero temperature value of $\varepsilon^{(\mathrm{QBT})}(0)$ in Eq. (49). In fact, although the integrand has a singularity at $q^2 = m^*\omega$, this singularity is not resolved at $T = 0$ due to the infrared cutoff provided from the Fermi-Dirac distribution, which limits the integration to $q > p_\mathrm{F}$. In striking contrast, for $T/E_\mathrm{F} > 0$ the whole range of momenta is supported due to the Fermi-Dirac distribution, and so every small $\omega/E_\mathrm{F} \neq 0$ contributes to the integral. In the curves shown in Fig. 6 we suppress this nonuniversal contribution by assuming $p^2/(2m^*\omega)$ to be small enough so that $\omega/E_\mathrm{F} \approx 0$, and so

$$\varepsilon^{(\mathrm{QBT})}(\omega) \approx \varepsilon^{(\mathrm{QBT})}(0) = \frac{2e^2}{\epsilon_0 m^*}\int_{\mathbf{q}} \frac{1 - n_\mathrm{F}\left(\frac{q^2}{2m^*} - \mu\right) - n_\mathrm{F}\left(\frac{q^2}{2m^*} + \mu\right)}{q^4/(m^*)^2}, \tag{75}$$

which is a universal function of T/E_F.

V. SUPERCONDUCTING STATE RESPONSE

In this section, after reviewing some general facts about superconductivity in Luttinger semimetals, we compute the intraband and interband contributions to the homogeneous optical response in the s-wave superconducting state. In particular, we derive explicit expressions for the QBT contribution to the Drude weight factor and superfluid density within RPA for both finite and zero chemical potential, which comprises weak and strong coupling superconductors. The result presented here are derived in Sec. S.IV of the SM [47].

A. Superconductivity in Luttinger semimetals

The complexity of the quadratic band touching point in Luttinger semimetals allows for a rich variety of possible superconducting ordered states. The corresponding Bogoliubov–de Gennes (BdG) Hamiltonian is given by

$$H_\mathrm{BdG}(\mathbf{p}) = \begin{pmatrix} \hat{H}(\mathbf{p}) - \mu & \hat{\Delta}(\mathbf{p}) \\ \hat{\Delta}(\mathbf{p})^\dagger & -\hat{H}(\mathbf{p})^T + \mu \end{pmatrix}, \tag{76}$$

with $\hat{H}(\mathbf{p})$ the Luttinger Hamiltonian from Eq. (3) and $\hat{\Delta}(\mathbf{p})$ a 4×4 gap matrix, so that the order parameter is given by $\langle\hat{\Delta}(\mathbf{p})\rangle$. In the simplest yet far from trivial case, the ordering is local and the gap matrix momentum independent. It can then be written as a sum of two parts according to

$$\langle\hat{\Delta}\rangle = (\Delta\mathbb{1}_4 + \phi_{ij}J_iJ_j)\mathcal{T}, \tag{77}$$

where $\mathcal{T}$ is the unitary part of the time-reversal operator (see Sec. S.I of the SM [47] for an explicit definition). The first term in Eq. (77) describes s-wave singlet superconducting order with order parameter Δ, whereas ϕ_{ij} is a symmetric and traceless complex tensor order parameter which represents Cooper pairs having spin 2 [27,52]. The onset of complex tensor order leads to very nontrivial momentum structures of the gap, having either line nodes or inflated Bogoliubov Fermi surfaces, that should manifest in nontrivial signatures in the optical conductivity. We do not explore this highly promising direction in this work, but refer to the next section for an outlook on aspects that should be addressed in the future.

For the present work we focus on the s-wave singlet superconducting order and assume without loss of generality that the order parameter is real, $\Delta \in \mathbb{R}$. The presence of a nonzero expectation value $\Delta \neq 0$ then leads to a full gap in the excitation spectrum. For $\mu = 0$, the opening of this gap requires sufficiently strong short-range interactions in the s-wave channel. At the critical coupling, the system features a quantum critical point at zero temperature, with non-Fermi liquid scaling of correlation functions and several other unusual scaling properties [18]. For $\mu \neq 0$, an infinitesimally small attraction in the s-wave channel is sufficient for ordering below an (exponentially small) critical temperature due to the Cooper instability. We therefore refer to the superconducting states that arise for $\mu = 0$ and $\mu \neq 0$ as strong coupling and weak coupling superconductors, respectively. In both cases the transition is of second order and the gap $\Delta(T)$ vanishes continuously at the critical temperature. The temperature dependence of the order parameter $\Delta(T)$ follows from the solution to an appropriate gap equation, which, however, requires knowledge of the coupling constant of the material. Since this quantity is generally not known in practice, we present our results as a function of independent parameters Δ and T, which comprises the same information and seems more accessible.

The RPA is known to yield an insufficient description of the optical response of superconductors in the single band case as it leads to expressions that violate gauge invariance. In particular, Eq. (26) for the longitudinal response is not satisfied by the RPA expressions and thus leads to the question on how to interpret the outcome of the approximate calculation. It turns out that the RPA expression for the transverse response can be used to define the optical conductivity, whereas gauge invariance of the longitudinal components is restored by including vertex corrections (see, e.g., Ref. [53] for a comprehensive discussion). We adopt this strategy for our analysis here as well and define the conductivity in the homogeneous case by

$$\sigma(\omega) := -\frac{4\pi\varepsilon_0}{i(\omega + i0)}K_\mathrm{T}(\omega, 0). \tag{78}$$

For small frequencies the conductivity behaves like [51,54]

$$\sigma_1(\omega) = \frac{\pi}{2}\delta(\omega)\frac{n'e^2}{m^*}, \tag{79}$$

$$\sigma_2(\omega) = \frac{n'e^2}{m^*\omega}, \tag{80}$$

with Drude weight factor

$$n' := \frac{4\pi\varepsilon_0 m^*}{e^2}\lim_{\omega\to 0} K_\mathrm{T}(\omega, 0). \tag{81}$$

Note that just like in Eq. (44) we define the δ-function to be restricted to $\omega \geqslant 0$, which explains the prefactor of $\frac{\pi}{2}$ when

going from Eq. (78) to (79). A quantity closely related to n' is the superfluid density defined by

$$n_{\rm s} := \frac{4\pi\varepsilon_0 m^*}{e^2}\lim_{p\to 0} K_{\rm T}(0,p). \tag{82}$$

The superfluid density allows for computing the London penetration depth.

B. *s*-wave singlet superconductor

Let us first discuss the superconductor with $\mu \neq 0$ and typically $\mu \gg \omega, T, \Delta$ for weak coupling, although we do not impose the latter restriction on our formulas. The intraband contribution to the conductivity is of the form of Eqs. (79) and (80) for all frequencies with Drude weight factor

$$n'^{(\rm intra)} = \int_{\mathbf{q}} \left(2 - \frac{\varepsilon_q}{E_q}[1-2n_{\rm F}(E_q)] + \frac{f_q}{F_q}[1-2n_{\rm F}(F_q)]\right), \tag{83}$$

with upper and lower band quasiparticle dispersions

$$\varepsilon_q = \frac{q^2}{2m^*} - \mu, \quad E_q = \sqrt{\varepsilon_q^2 + \Delta^2}, \tag{84}$$

$$f_q = -\frac{q^2}{2m^*} - \mu, \quad F_q = \sqrt{f_q^2 + \Delta^2}. \tag{85}$$

Note that the paramagnetic term $K_{\rm T}^{(\rm p,intra)}(\omega,0)$ vanishes within RPA, and so only the diamagnetic term contributes to Eq. (81). Furthermore, for $\Delta \neq 0$ the cancellation between diamagnetic and paramagnetic contribution to $\lim_{p\to 0} K_{\rm T}^{(\rm intra)}(0,p)$ is not perfect, and we obtain a finite contribution to the superfluid density given by

$$n_{\rm s}^{(\rm intra)} = n'^{(\rm intra)} + \frac{4}{3}\int_{\mathbf{q}} \frac{q^2}{2m^*}\left[\frac{\partial}{\partial E_q} n_{\rm F}(E_q) + \frac{\partial}{\partial F_q} n_{\rm F}(F_q)\right]. \tag{86}$$

Notice that the term in the second line is negative and so we have $n'^{(\rm intra)} \geqslant n_{\rm s}^{(\rm intra)}$, with equality at zero temperature. For vanishing gap, $\Delta \to 0$, the intraband contribution to the Drude weight reproduces n from Eq. (33) and the superfluid density vanishes.

The QBT contribution to the optical conductivity is given by

$$\begin{aligned}\sigma^{(\rm QBT)}(\omega) = &-\frac{e^2/m^*}{i(\omega+i0)}\int_{\mathbf{q}} \frac{1}{(\omega+i0)^4 - 4(\omega+i0)^2\left[\frac{q^4}{(2m^*)^2} + \mu^2 + \Delta^2\right] + 16\mu^2\frac{q^4}{(2m^*)^2}} \\ &\times \left\{\left[\omega^4\varepsilon_q - 4\omega^2\varepsilon_q(\mu^2+\Delta^2) + 16\mu\Delta^2\frac{q^4}{(2m^*)^2}\right]\frac{1}{E_q}[1-2n_{\rm F}(E_q)]\right. \\ &\left. -\left[\omega^4 f_q - 4\omega^2 f_q(\mu^2+\Delta^2) + 16\mu\Delta^2\frac{q^4}{(2m^*)^2}\right]\frac{1}{F_q}[1-2n_{\rm F}(F_q)]\right\}.\end{aligned} \tag{87}$$

For $\omega \gg \Delta$ the response function resembles the features of the normal state response, whereas for smaller $\omega \sim \Delta$ the conductivity has the form of Eqs. (79) and (80) with

$$n'^{(\rm QBT)} = \frac{\Delta^2}{\mu}\int_{\mathbf{q}}\left(\frac{1}{E_q}[1-2n_{\rm F}(E_q)] - \frac{1}{F_q}[1-2n_{\rm F}(F_q)]\right). \tag{88}$$

This expression is positive for either sign of μ. Remarkably, the QBT contributions to n' and $n_{\rm s}$ coincide for all temperatures,

$$n'^{(\rm QBT)} = n_{\rm s}^{(\rm QBT)} \quad \text{for } \mu \neq 0, \tag{89}$$

due to

$$\lim_{p\to 0} K_{\rm T}^{(\rm QBT)}(0,p) = \lim_{\omega\to 0} K_{\rm T}^{(\rm QBT)}(\omega,0) \tag{90}$$

for $\mu \neq 0$. This also holds in the normal phase, where $n'^{(\rm QBT)} = n_{\rm s}^{(\rm QBT)} = 0$. Indeed, the normal state QBT contribution is finite for $\omega = 0$ and $\mu \neq 0$, and the singular part of the optical response purely stems from the intraband terms. Note that both the intraband and QBT contributions to the Drude weight and superfluid density satisfy $n' \geqslant n_{\rm s}$. (This is also true in the case of $\mu = 0$ discussed in the next section.) Consequently, there is no violation of the necessary requirement that the superfluid density must not exceed the density of charge carriers. In Fig. 7 we show the crossover of the conductivity from the normal state behavior for $\omega \gg \Delta$ to the superfluid behavior for small $\omega \sim \Delta$.

Equation (89) implies the usual exponentially weak temperature dependence $\sim e^{-\Delta/T}$ of the superfluid density and penetration depth for small temperatures that is characteristic for *s*-wave superconductors. In particular, for small temperatures $T \ll T_{\rm c}$ such as in the experiments of Ref. [6], the temperature dependence of the gap $\Delta_0(T)$ that solves the corresponding gap equation is weak for an *s*-wave superconductor and so we can assume $\Delta_0(T) \approx \Delta_0(0)$ to be constant at low temperatures.

C. Strong coupling superconductor

A conceptually interesting limit of the formulas from the previous section consists in considering the case of $\mu = 0$. Such a superconductor with $\Delta \neq 0$ can obviously not be caused by the Cooper instability and requires very strong coupling between fermions, but as a theoretic limit it is still worthwhile to study. The gap Δ then constitutes the only energy scale of the system at zero temperature, and thus is the only quantity that alters the universal limit $\varepsilon(\omega) = \frac{e^2}{4\pi\epsilon_0}\sqrt{\frac{m^*}{\omega}}(1+i)$ in Eq. (48). Note that the strong

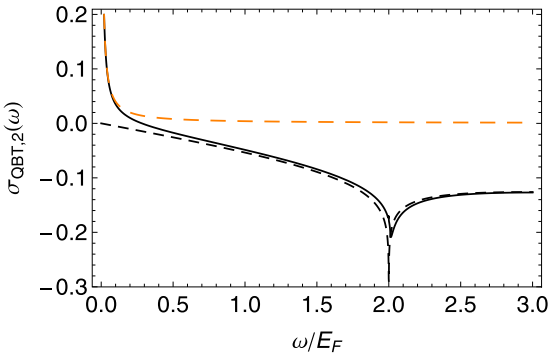

FIG. 7. Crossover from normal to superfluid behavior in the QBT contribution to the optical conductivity at $T = 0$. The black solid line shows the result in the s-wave superconducting case with gap $\Delta/E_{\mathrm{F}} = 0.1$, whereas the black dashed line shows the corresponding normal state result. The orange long-dashed line corresponds to the low-frequency behavior $n'^{(\mathrm{QBT})}e^2/(m^*\omega)$ with QBT contribution to the Drude weight from Eq. (88). We observe that $\sigma_2(\omega)$ changes sign and so connects the negative normal state limit for $\omega \gg \Delta$ to the positive Drude like scaling at low frequencies $\omega \sim \Delta$. The same behavior is found in the strong coupling case with $\mu = 0$, see Fig. 8.

coupling required here to form the superconductor is reminiscent of the critical coupling for the existence of a bound state or dimer of two-component fermions in vacuum (i.e., for $\mu = 0$) [55,56], which leads to the phenomenology of the BCS-BEC crossover for $\mu > 0$ and is realized with Feshbach resonances in ultracold Fermi gases [57–59].

The transverse response function for $\mu = 0$ is given by

$$K_{\mathrm{T}}^{(\mathrm{QBT})}(\omega, 0) = \frac{e^2(4\Delta^2 - \omega^2)}{2\pi\epsilon_0 m^*} \int_{\mathbf{q}} \frac{\frac{q^2}{2m^*}[1 - 2n_{\mathrm{F}}(E_q)]}{E_q\big[-(\omega + i0)^2 + 4E_q^2\big]}, \tag{91}$$

with $E_q = \sqrt{q^4/(2m^*)^2 + \Delta^2}$. We define $\sigma(\omega)$ through $K_{\mathrm{T}}^{(\mathrm{QBT})}(\omega, 0)$ by Eq. (78). The corresponding optical conductivity is plotted in Fig. 8 for a representative set of temperatures. The real part is given by

$$\sigma_1^{(\mathrm{QBT})}(\omega) = \frac{\pi}{2}\delta(\omega)\frac{n'^{(\mathrm{QBT})}e^2}{m^*} + \frac{e^2}{4\pi}\theta(\omega - 2\Delta)\sqrt{m^*\omega} \times \left(1 - \frac{4\Delta^2}{\omega^2}\right)^{5/4}[1 - 2n_{\mathrm{F}}(\omega/2)], \tag{92}$$

with Drude weight factor

$$n'^{(\mathrm{QBT})} = 2\Delta^2 \int_{\mathbf{q}} \frac{q^2}{2m^*}\frac{1}{E_q^3}[1 - 2n_{\mathrm{F}}(E_q)]. \tag{93}$$

Similarly, the imaginary part for small ω follows Eq. (80) with $n'^{(\mathrm{QBT})}$. Importantly, the conductivity is finite at $\omega = 2\Delta$. The contribution to the superfluid density is given by

$$n_{\mathrm{s}}^{(\mathrm{QBT})} = 2\Delta^2 \int_{\mathbf{q}} \frac{q^2}{2m^*}\left(\frac{1}{E_q^3}[1 - 2n_{\mathrm{F}}(E_q)] + \frac{2}{E_q^2}\frac{\partial}{\partial E_q}n_{\mathrm{F}}(E_q)\right), \tag{94}$$

which is the $\mu \to 0$ limit of Eq. (88). We conclude that $n'^{(\mathrm{QBT})} > n_{\mathrm{s}}^{(\mathrm{QBT})}$ for the superconductor with $\mu = 0$ at finite temperature. At zero temperature we find the explicit expression

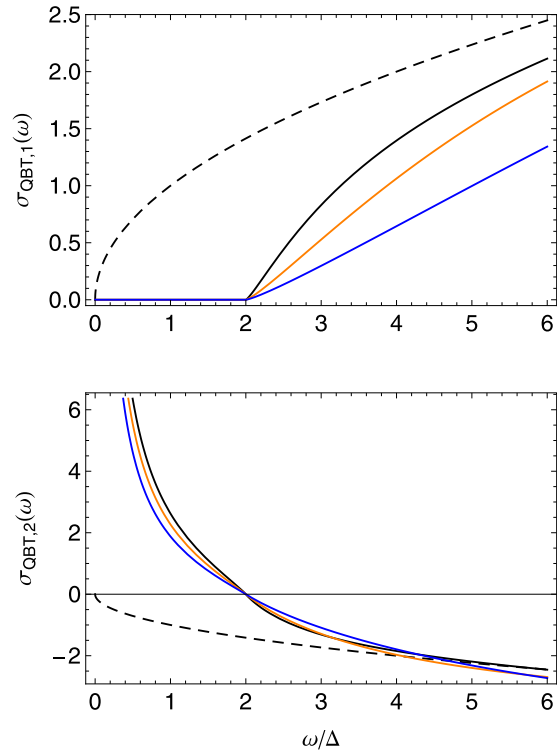

FIG. 8. QBT contribution to the optical conductivity of a strong coupling superconductor with $\mu = 0$. The solid lines in the upper and lower panel show the real and imaginary part, respectively, for $T = 0$ (black), $T/\Delta = 1$ (orange), and $T/\Delta = 2$ (blue). We only plot the regular part of $\sigma_1(\omega)$, see Eq. (92). The dashed lines show the corresponding normal state limit $\sigma(\omega) = \frac{e^2}{4\pi}\sqrt{m^*\omega}(1 - i)$ for $\mu = T = 0$. The real part displays threshold behavior at $\omega = 2\Delta$, whereas the imaginary part changes sign at this frequency. As a result, the imaginary part is negative for large frequencies—in agreement with the negative normal state limit—and it is positive with Drude-like behavior as in Eq. (80) for small frequencies.

$$n'^{(\mathrm{QBT})} = n_{\mathrm{s}}^{(\mathrm{QBT})} = \frac{2\Gamma\left(\frac{5}{4}\right)^2}{\pi^{5/2}}(2m^*\Delta)^{3/2}, \tag{95}$$

with Euler's Γ-function $\Gamma(z)$.

The case of $\mu = 0$ allows us to make the shortcomings of the RPA with respect to gauge invariance particularly visible. In fact, Eq. (26) implies that gauge invariance requires

$$K_{\mathrm{L}}^{(\mathrm{QBT})}(\omega, 0) \stackrel{!}{=} -\omega^2 Z_{\mathrm{QBT}}(\omega). \tag{96}$$

However, the RPA equations for $\mu = 0$ result in

$$K_{\mathrm{L}}^{(\mathrm{QBT,RPA})}(\omega, 0) = (4\Delta^2 - \omega^2)Z_{\mathrm{QBT}}^{(\mathrm{RPA})}(\omega), \tag{97}$$

which also holds at finite temperature, see Eq. (S.336) in the SM [47]. We added the superscript RPA to emphasize that these quantities deviate from the physical or measurable observable which satisfy gauge invariance. If we use $Z_{\mathrm{QBT}}^{(\mathrm{RPA})}(\omega)$ to define a conductivity by means of

$\tilde{\sigma}^{(\mathrm{QBT})}(\omega) := -4\pi\epsilon_0 i\omega Z^{(\mathrm{RPA})}_{\mathrm{QBT}}(\omega)$, then

$$\tilde{\sigma}^{(\mathrm{QBT})}(\omega) = \frac{\omega^2}{\omega^2 - 4\Delta^2}\sigma^{(\mathrm{QBT})}(\omega). \tag{98}$$

This quantity differs from $\sigma^{(\mathrm{QBT})}(\omega)$ in two crucial aspects: First, the imaginary part $\tilde{\sigma}_2^{(\mathrm{QBT})}(\omega)$ has a divergence at $\omega = 2\Delta$. Second, for $\omega \to 0$ we have $\tilde{\sigma}_2^{(\mathrm{QBT})}(\omega) \sim -\frac{n'^{(\mathrm{QBT})}e^2}{4m^*\Delta^2}\omega \to 0$, and so there is no Drude-like behavior at small frequencies. We leave it for future work to study how gauge invariance can be restored by including corrections that go beyond the RPA.

VI. SUMMARY AND OUTLOOK

In this work we have explored the optical conductivity of Luttinger semimetals in the normal and superconducting states. The motivation for this investigation is, on the one hand, recent experiments on the optical properties of pyrochlore iridates and half-Heusler superconductors, and, on the other hand, the recent theoretical discovery of a plethora of possible novel unconventional superconducting orders in QBT materials. Thus, although the optical properties of QBT systems in the normal state have been studied before in the context of α-Sn [39,60,61], these current experimental and theoretical developments call for a more refined understanding of the electromagnetic properties of Luttinger semimetals, especially when interactions are strong or the material is in the superconducting state.

Our analysis has been built on the RPA, which constitutes the natural first step towards understanding the optical response functions. Crucially, in our analysis we have kept the full internal 4×4 structure of the Luttinger Hamiltonian, which results in considerably unwieldy computations, but allows us to identify both intraband and interband contributions in an unbiased way. In the normal state, the genuine QBT contribution from interband transitions is large at low frequencies in the homogeneous limit, and it dominates the quasistatic limit. Furthermore, in the superconducting state the contribution from interband transitions is important to capture effects that are absent for single band systems. In particular, this includes Bogoliubov Fermi surfaces of certain superconducting orders in Luttinger semimetals. In the present work we have derived the general expression for the optical response in the superconducting state and applied it to the s-wave singlet superconducting case, where we find a genuine QBT contribution to the superfluid density and Drude weight.

The results that are shown in the main text of this work are either analytically evaluated or in terms of simple one-dimensional integrals. To achieve this simplicity we have restricted the presentation to the homogeneous and quasistatic limits, which are by far the most practically relevant ones. However, the full frequency and momentum dependence for the normal state response can be inferred from Eq. (S.225) for $K_{\mathrm{T}}^{(\mathrm{QBT})}$ and Eq. (S.262) for χ_{QBT} in the SM [47]. In particular, in Sec. S.III.C [47] we show that the longitudinal QBT component satisfies the gauge invariance condition (26) for all values of ω and p, and so $K_{\mathrm{L}}^{(\mathrm{QBT})}$ can be deduced from χ_{QBT}. This leaves us with a consistent picture in the normal state, where the L component of $\varepsilon_{ij}^{(\mathrm{QBT})}$ can be computed from either the density or current response functions.

The consistent picture of the normal state response is absent at the RPA level in the superconducting state, where $\chi^{(\mathrm{RPA})}$ and $K_{\mathrm{L}}^{(\mathrm{RPA})}$ do not satisfy the gauge invariance condition (26). Consequently an ambiguity arises when defining, for instance, the homogeneous conductivity $\sigma(\omega)$ from either of the two functions. This is a well-known feature for the single parabolic band, and a way around consists in either including vertex corrections to restore gauge invariance, or to use the transverse component of the current response function to define $\sigma(\omega)$. We applied the second strategy here to infer the QBT contribution in the superconducting state, which gives the conveniently short expression for the conductivity in Eq. (87), but since we have not considered the effect of vertex corrections it is too early to conclude whether this approach is correct. For the superconductor with $\mu = 0$ we discussed in Eqs. (96)–(98) how the conductivity in the homogeneous limit differs qualitatively when defined from either K_{T} or χ.

The present work can be extended in several directions, out of which we name a few in the following. One application in the normal and superconducting state is to quantify the anomalous skin effect in Luttinger semimetals, both in the normal and superconducting phase. In fact, the quasistatic limit $q^2/(2m^*) \ll \omega \ll vp$ considered above is typically referred to as an "extreme anomalous limit" in superconductors. The corresponding intraband contribution from the upper band has been derived in the seminal works by Mattis, Bardeen [62], and by Abrikosov, Gor'kov, and Khalatnikov [63]. Since we have found the normal state response in the quasistatic limit to be dominated by the QBT contribution, the behavior of Luttinger semimetals is likely to be distinctively different from single band systems in the anomalous limit, with striking observable effects in both the normal and superconducting states.

The optical response in other than s-wave singlet superconducting states can be obtained by using the general expression for the fermion propagator in the mean-field approximation in Eq. (S.102) in the SM [47] with a suitable gap matrix $\hat{\Delta}$ and repeating the steps outlined in Sec. S.IV. In fact, two very interesting and important cases are covered by the local gap matrix from Eq. (77) with $\phi_{ij} \neq 0$: (i) By choosing a real tensor $\phi \neq 0$, the effect of nematic superconducting order on the optical response can be probed. In particular, the nematic orders feature line nodes of the gap and a spontaneous breaking of rotation symmetry. It will be exciting to see how both effects manifest in the optical response and how they relate to the measurements on half-Heusler superconductors. (ii) Choosing a genuinely complex tensor ϕ such that $\mathrm{tr}(\phi^2) = 0$ we can study superconducting orders that spontaneously break time-reversal symmetry and lead to Bogoliubov surfaces in the gap [23,45,46]. Again, this very intriguing finding calls to be explored within the framework of electromagnetic response functions.

In order to study the effects of strong interactions and critical fluctuations on the optical response of Luttinger semimetals, it is mandatory to go beyond the RPA. First, Coulomb interactions between the electrons are relevant and famously lead to Abrikosov's non-Fermi liquid scaling of correlation functions (at least within certain regimes). Second, in the

vicinity of a quantum critical point, as may be the case for Pr-227 as discussed in the Introduction, critical fluctuations of the order parameter can modify the nature of fermionic excitations. To solve such a setup self-consistently is a very challenging task and worth exploring. In a less ambitious attempt, however, it will also be interesting to assume that the mentioned strong interactions merely result in a renormalization of the fermion propagator and then use the renormalized propagator to estimate the optical response function from the fermionic one-loop diagram. Furthermore, the infrared regime can be addressed self-consistently by a scaling or renormalization group approach to infer the scaling exponents. These theoretical studies will help to design and interpret future experiments on Luttinger semimetals.

ACKNOWLEDGMENTS

The author thanks Igor Herbut and Steve Dodge for inspiring discussions. This work was supported by the Natural Sciences and Engineering Research Council of Canada, the DoE BES Materials and Chemical Sciences Research for Quantum Information Science program, NSF Ideas Lab on Quantum Computing, DoE ASCR Quantum Testbed Pathfinder program, ARO MURI, ARL CDQI, and NSF PFC at JQI.

[1] X.-L. Qi and S.-C. Zhang, Topological insulators and superconductors, Rev. Mod. Phys. **83**, 1057 (2011).

[2] W. Witczak-Krempa, G. Chen, Y. B. Kim, and L. Balents, Correlated quantum phenomena in the strong spin-orbit regime, Annu. Rev. Condens. Matter Phys. **5**, 57 (2014).

[3] M. Smidman, M. B. Salamon, H. Q. Yuan, and D. F. Agterberg, Superconductivity and spin-orbit coupling in non-centrosymmetric materials: a review, Rep. Prog. Phys. **80**, 036501 (2017).

[4] S. Chadov, X. Qi, J. Kübler, G. H. Fecher, C. Felser, and S. C. Zhang, Tunable multifunctional topological insulators in ternary Heusler compounds, Nat. Mater. **9**, 541 (2010).

[5] B. Cheng, T. Ohtsuki, D. Chaudhuri, S. Nakatsuji, M. Lippmaa, and N. P. Armitage, Dielectric anomalies and interactions in the three-dimensional quadratic band touching Luttinger semimetal $Pr_2Ir_2O_7$, Nat. Commun. **8**, 2097 (2017).

[6] H. Kim, K. Wang, Y. Nakajima, R. Hu, S. Ziemak, P. Syers, L. Wang, H. Hodovanets, J. D. Denlinger, P. M. R. Brydon, D. F. Agterberg, M. A. Tanatar, R. Prozorov, and J. Paglione, Beyond triplet: Unconventional superconductivity in a spin-3/2 topological semimetal, Sci. Adv. **4**, eaao4513 (2018).

[7] A. A. Abrikosov, Calculation of critical indices of zero-gap semiconductors, Sov. Phys. JETP **39** , 709 (1974).

[8] A. A. Abrikosov and S. D. Beneslavskii, Possible existence of substances intermediate between metals and dielectrics, Sov. Phys. JETP **32**, 699 (1971).

[9] E.-G. Moon, C. Xu, Y. B. Kim, and L. Balents, Non-Fermi-Liquid and Topological States with Strong Spin-Orbit Coupling, Phys. Rev. Lett. **111**, 206401 (2013).

[10] I. F. Herbut and L. Janssen, Topological Mott Insulator in Three-Dimensional Systems with Quadratic Band Touching, Phys. Rev. Lett. **113**, 106401 (2014).

[11] L. Janssen and I. F. Herbut, Excitonic instability of three-dimensional gapless semiconductors: Large-N theory, Phys. Rev. B **93**, 165109 (2016).

[12] L. Janssen and I. F. Herbut, Phase diagram of electronic systems with quadratic Fermi nodes in $2 < d < 4$: $2 + \epsilon$ expansion, $4 - \epsilon$ expansion, and functional renormalization group, Phys. Rev. B **95**, 075101 (2017).

[13] I. Mandal and R. M. Nandkishore, Interplay of Coulomb interactions and disorder in three-dimensional quadratic band crossings without time-reversal symmetry and with unequal masses for conduction and valence bands, Phys. Rev. B **97**, 125121 (2018).

[14] W. Witczak-Krempa and Y. B. Kim, Topological and magnetic phases of interacting electrons in the pyrochlore iridates, Phys. Rev. B **85**, 045124 (2012).

[15] L. Savary, E.-G. Moon, and L. Balents, New Type of Quantum Criticality in the Pyrochlore Iridates, Phys. Rev. X **4**, 041027 (2014).

[16] L. Janssen and I. F. Herbut, Nematic quantum criticality in three-dimensional Fermi system with quadratic band touching, Phys. Rev. B **92**, 045117 (2015).

[17] J. M. Murray, O. Vafek, and L. Balents, Incommensurate spin density wave at a ferromagnetic quantum critical point in a three-dimensional parabolic semimetal, Phys. Rev. B **92**, 035137 (2015).

[18] I. Boettcher and I. F. Herbut, Superconducting quantum criticality in three-dimensional Luttinger semimetals, Phys. Rev. B **93**, 205138 (2016).

[19] M. Meinert, Unconventional Superconductivity in YPtBi and Related Topological Semimetals, Phys. Rev. Lett. **116**, 137001 (2016).

[20] P. M. R. Brydon, L. Wang, M. Weinert, and D. F. Agterberg, Pairing of $j = 3/2$ Fermions in Half-Heusler Superconductors, Phys. Rev. Lett. **116**, 177001 (2016).

[21] P. Goswami, B. Roy, and S. Das Sarma, Competing orders and topology in the global phase diagram of pyrochlore iridates, Phys. Rev. B **95**, 085120 (2017).

[22] I. Boettcher and I. F. Herbut, Anisotropy induces non-Fermi-liquid behavior and nematic magnetic order in three-dimensional Luttinger semimetals, Phys. Rev. B **95**, 075149 (2017).

[23] D. F. Agterberg, P. M. R. Brydon, and C. Timm, Bogoliubov Fermi Surfaces in Superconductors with Broken Time-Reversal Symmetry, Phys. Rev. Lett. **118**, 127001 (2017).

[24] S. A. A. Ghorashi, S. Davis, and M. S. Foster, Disorder-enhanced topological protection and universal quantum criticality in a spin-$\frac{3}{2}$ topological superconductor, Phys. Rev. B **95**, 144503 (2017).

[25] W. Yang, T. Xiang, and C. Wu, Majorana surface modes of nodal topological pairings in spin-$\frac{3}{2}$ semimetals, Phys. Rev. B **96**, 144514 (2017).

[26] L. Savary, J. Ruhman, J. W. F. Venderbos, L. Fu, and P. A. Lee, Superconductivity in three-dimensional spin-orbit coupled semimetals, Phys. Rev. B **96**, 214514 (2017).

[27] I. Boettcher and I. F. Herbut, Unconventional Superconductivity in Luttinger Semimetals: Theory of Complex Tensor Order and

the Emergence of the Uniaxial Nematic State, Phys. Rev. Lett. **120**, 057002 (2018).

[28] J. W. F. Venderbos, L. Savary, J. Ruhman, P. A. Lee, and L. Fu, Pairing States of Spin-$\frac{3}{2}$ Fermions: Symmetry-Enforced Topological Gap Functions, Phys. Rev. X **8**, 011029 (2018).

[29] S. A. A. Ghorashi, P. Hosur, and C.-S. Ting, Irradiated three-dimensional Luttinger semimetal: A factory for engineering Weyl semimetals, Phys. Rev. B **97**, 205402 (2018).

[30] I. Mandal, Fate of superconductivity in three-dimensional disordered Luttinger semimetals, Ann. Phys. **392**, 179 (2018).

[31] J. Yu and C.-X. Liu, Singlet-quintet mixing in spin-orbit coupled superconductors with $j = \frac{3}{2}$ fermions, Phys. Rev. B **98**, 104514 (2018).

[32] X.-P. Yao and G. Chen, $Pr_2Ir_2O_7$: When Luttinger Semimetal Meets Melko-Hertog-Gingras Spin Ice State, Phys. Rev. X **8**, 041039 (2018).

[33] B. Roy, S. A. A. Ghorashi, M. S. Foster, and A. H. Nevidomskyy, Topological superconductivity of spin-3/2 carriers in a three-dimensional doped luttinger semimetal, Phys. Rev. B **99**, 054505 (2019).

[34] G. Sim, A. Mishra, M. Jip Park, Y. B. Kim, G. Y. Cho, and S. Lee, Topological d+s wave superconductors in a multi-orbital quadratic band touching system, arXiv:1811.04046.

[35] A. Szabo, R. Moessner, and B. Roy, Interacting spin-3/2 fermions in a Luttinger (semi)metal: Competing phases and their selection in the global phase diagram, arXiv:1811.12415.

[36] T. Kondo, M. Nakayama, R. Chen, J. J. Ishikawa, E.-G. Moon, T. Yamamoto, Y. Ota, W. Malaeb, H. Kanai, Y. Nakashima, Y. Ishida, R. Yoshida, H. Yamamoto, M. Matsunami, S. Kimura, N. Inami, K. Ono, H. Kumigashira, S. Nakatsuji, L. Balents, and S. Shin, Quadratic Fermi node in a 3D strongly correlated semimetal, Nat. Commun. **6**, 10042 (2015).

[37] M. Nakayama, T. Kondo, Z. Tian, J. J. Ishikawa, M. Halim, C. Bareille, W. Malaeb, K. Kuroda, T. Tomita, S. Ideta, K. Tanaka, M. Matsunami, S. Kimura, N. Inami, K. Ono, H. Kumigashira, L. Balents, S. Nakatsuji, and S. Shin, Slater to Mott Crossover in the Metal to Insulator Transition of $Nd_2Ir_2O_7$, Phys. Rev. Lett. **117**, 056403 (2016).

[38] T. Liang, T. H. Hsieh, J. J. Ishikawa, S. Nakatsuji, L. Fu, and N. P. Ong, Orthogonal magnetization and symmetry breaking in pyrochlore iridate $Eu_2Ir_2O_7$, Nat. Phys. **13**, 599 (2017).

[39] J. G. Broerman, Random-phase-approximation dielectric function of *a*-Sn in the far infrared, Phys. Rev. B **5**, 397 (1972).

[40] I. Mandal, Search for plasmons in isotropic Luttinger semimetals, arXiv:1810.06574.

[41] N. P. Butch, P. Syers, K. Kirshenbaum, A. P. Hope, and J. Paglione, Superconductivity in the topological semimetal YPtBi, Phys. Rev. B **84**, 220504(R) (2011).

[42] T. V. Bay, T. Naka, Y. K. Huang, and A. de Visser, Superconductivity in noncentrosymmetric YPtBi under pressure, Phys. Rev. B **86**, 064515 (2012).

[43] T. V. Bay, M. Jackson, C. Paulsen, C. Baines, A. Amato, T. Orvis, M. C. Aronson, Y. K. Huang, and A. de Visser, Low field magnetic response of the non-centrosymmetric superconductor YPtBi, Solid State Commun. **183**, 13 (2014).

[44] J. M. Luttinger, Quantum theory of cyclotron resonance in semiconductors: General theory, Phys. Rev. **102**, 1030 (1956).

[45] C. Timm, A. P. Schnyder, D. F. Agterberg, and P. M. R. Brydon, Inflated nodes and surface states in superconducting half-Heusler compounds, Phys. Rev. B **96**, 094526 (2017).

[46] P. M. R. Brydon, D. F. Agterberg, H. Menke, and C. Timm, Bogoliubov Fermi surfaces: General theory, magnetic order, and topology, Phys. Rev. B **98**, 224509 (2018).

[47] See Supplemental Material at http://link.aps.org/supplemental/10.1103/PhysRevB.99.125146 for algebraic conventions, a self-contained derivation of response functions from the path integral, and the computation of response functions for QBT systems in the normal and superconducting states.

[48] Yu. A. Ill'inski and L. V. Keldysh, *Electromagnetic Response of Material Media* (Plenum, New York, 1994).

[49] M. Dressel and G. Grüner, *Electrodynamics of Solids: Optical Properties of Electrons in Matter* (Cambridge University Press, Cambridge, 2002).

[50] A. Altland and B. Simons, *Condensed Matter Field Theory* (Cambridge University Press, Cambridge, 2010).

[51] M. Tinkham, *Introduction to Superconductivity* (McGraw Hill, New York, 1996).

[52] I. Boettcher and I. F. Herbut, Critical phenomena at the complex tensor ordering phase transition, Phys. Rev. B **97**, 064504 (2018).

[53] G. Seibold, L. Benfatto, and C. Castellani, Application of the Mattis-Bardeen theory in strongly disordered superconductors, Phys. Rev. B **96**, 144507 (2017).

[54] M. Dressel, Electrodynamics of metallic superconductors, Adv. Condens. Matter Phys. **2013**, 104379 (2013).

[55] S. Diehl and C. Wetterich, Universality in phase transitions for ultracold fermionic atoms, Phys. Rev. A **73**, 033615 (2006).

[56] P. Nikolic and S. Sachdev, Renormalization-group fixed points, universal phase diagram, and $1/N$ expansion for quantum liquids with interactions near the unitarity limit, Phys. Rev. A **75**, 033608 (2007).

[57] W. Zwerger, Ed., *The BCS-BEC Crossover and the Unitary Fermi Gas* (Springer, Berlin, 2012).

[58] I. Boettcher, J. M. Pawlowski, and S. Diehl, Ultracold atoms and the functional renormalization group, Nucl. Phys. B Proc. Suppl. **228**, 63 (2012).

[59] I. Boettcher, J. M. Pawlowski, and C. Wetterich, Critical temperature and superfluid gap of the unitary Fermi gas from functional renormalization, Phys. Rev. A **89**, 053630 (2014).

[60] L. Liu and D. Brust, Static Dielectric Function of a Zero-Gap Semiconductor, Phys. Rev. Lett. **20**, 651 (1968).

[61] J. G. Broerman, Temperature Dependence of the Static Dielectric Constant of a Symmetry-Induced Zero-Gap Semiconductor, Phys. Rev. Lett. **25**, 1658 (1970).

[62] D. C. Mattis and J. Bardeen, Theory of the anomalous skin effect in normal and superconducting metals, Phys. Rev. **111**, 412 (1958).

[63] A. A. Abrikosov, L. P. Gor'kov, and I. M. Khalatnikov, A superconductor in a high frequency field, Sov. Phys. JETP **35**, 182 (1959).